Laser induced fluorescence of xenon ions in a magnetized plasma

I. A. Biloiu[1], E. E. Scime[1], and C. Biloiu[1,2]

[1] *West Virginia University, Physics Department, Morgantown, WV 26506, USA*
[2] *Varian Semiconductor Equipment Associates, 35 Dory Road, Gloucester, MA 01930, USA*

A complete analysis of the three level Xe^+ laser induced fluorescence (LIF) scheme, 5d $^4D_{7/2} \rightarrow$ 6p $^4P_{5/2} \rightarrow$ 6s $^4P_{5/2}$, in the presence of an external magnetic field is presented. Isotopic, nuclear spin, and Zeeman splitting effects on ion velocity distribution function (ivdf) measurements are evaluated and the impact on ion velocity and ion temperature determination quantified. It is shown that by neglecting Zeeman splitting, the precision of ion velocity determination remains less than a few tens of m/s. However, the complex hyperfine and Zeeman splittings make precise ion temperature determination problematic. Based on measurements of the perpendicular Xe^+ ivdf in a stationary plasma, a rest frame wave number of 16521.332 cm^{-1} for the Xe^+ 605.2781 nm absorption line is reported. Measurements of the parallel Xe^+ ivdf in a helicon plasma ~100 cm downstream from the antenna evidence an axial ambipolar electric field of ~2.5 V/m independent of the applied rf power.

1. Introduction

Due to its sensitivity, high spatial (few mm^3) and temporal (microseconds) resolution, and non-invasive character, laser induced fluorescence (LIF) is an indispensable tool in plasma diagnosis.

For plasma thruster characterization, a quantitative assessment is the value of the specific impulse $I = v/g$, where v is the speed of the ejected ion and g = 9.8 ms^{-2} the gravitational acceleration. Because of its heavy weight and low ionization potential, xenon is the gas of choice for plasma thruster applications. In the case of Hall thrusters, magnetic fields are used to eject ions and accelerate a spacecraft. Therefore, developing LIF schemes that non-invasively allow measurement of the emitted Xe^+ ion velocity distribution function (ivdf) is of great interest for plasma propulsion studies [1, 2].

2. Xe ion LIF

One of the 3-level Xe ion LIF schemes accessible with a tunable dye laser is shown in Figure 1a. The laser wavelength is tuned to 605.278 nm (vacuum wavelength) to pump Xe^+ from the metastable 5d $^4D_{7/2}$ state to the excited 6p $^4P_{5/2}$ state. Ions in the 6p $^4P_{5/2}$ state (τ = 7.8 ns lifetime [3]) decay to 6s $^4P_{5/2}$ state, emitting a 529.369 nm photon (vacuum wavelength). Since the first state is metastable ($\tau \approx$ 200 ms lifetime [4]), the homogenous line width ($\Delta E \approx \hbar/\tau$) of the absorption process is dominated by the natural linewidth of the 6p $^4P_{5/2}$ level. The resultant 2×10^{-2} GHz linewidth is extremely small compared to typical Doppler broadened linewidths for Xe^+; approximately 0.53 GHz for $^{132}Xe^+$ at room temperature. The fine structure splitting of Xe^+ levels results in a large number of absorption lines, closely spaced in wavelength.

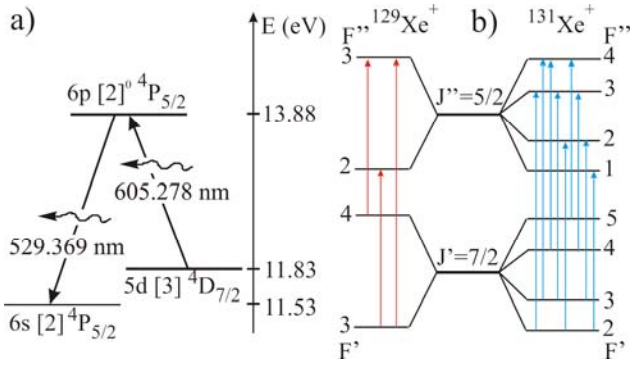

FIG. 1. a) Three-level Xe^+ LIF scheme; b) hyperfine structure of 605.278 nm line of the odd isotopes due to nuclear spin splitting.

The hyperfine structure of Xe^+ is a nuclear effect and includes the effects of mass (isotope effect) and nuclear spin (caused by the coupling between the nuclear spin **I** and the total electronic angular momentum **J**). Because the hyperfine splitting is significant (see Fig. 1.b), the absorption spectrum line shape in Xe^+ LIF is a convolution of the hyperfine splitting and Doppler broadening.

2.1. Isotopic splitting

Xenon has a rich spectrum of isotopes, five of them having natural abundances of 10% or more; with $^{129}Xe^+$ and $^{132}Xe^+$ having the largest abundances of 26.4% and 26.9% , respectively [5]. Each of the isotopes causes a shift of the xenon ion energy levels. The shifts range from a few tens to a few hundreds of MHz [6]. Figure 2 depicts the naturally-occurring xenon isotopic abundances and shifts in the 5d $^4D_{7/2} \rightarrow$ 6p $^4P_{5/2}$ transition relative to same transition in $^{132}Xe^+$.

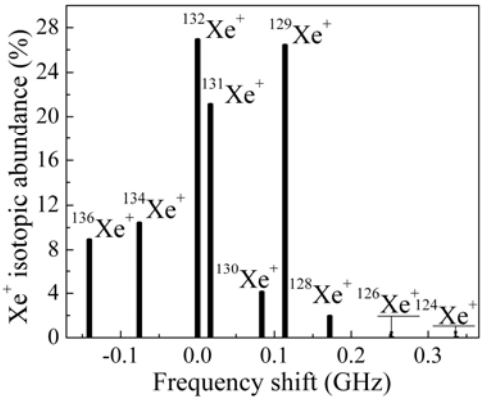

FIG. 2. Xe^+ isotopic abundance and frequency shifts relative to $^{132}Xe^+$ for the 5d $^4D_{7/2} \rightarrow$ 6p $^4P_{5/2}$ transition [5].

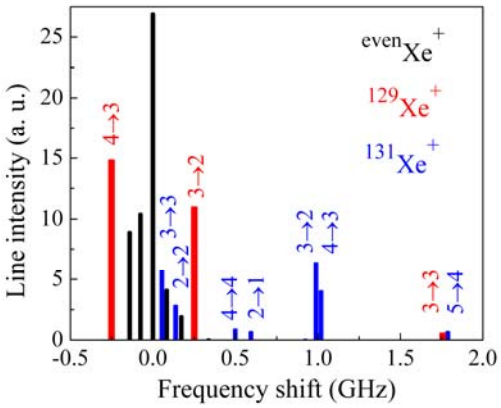

FIG. 3. Xe^+ 5d $^4D_{7/2} \rightarrow$ 6p $^4P_{5/2}$ hyperfine line splitting. The transition label on each vertical line is $F' \rightarrow F''$.

2.2. Nuclear spin splitting

Of the nine isotopes of xenon, seven have an even atomic mass. Thus, they have a nuclear spin of $\boldsymbol{I} = 0$ and do not contribute to the nuclear spin splitting. The remaining two isotopes have odd atomic masses and non-zero nuclear spin quantum numbers I. While the lighter isotope, $^{129}Xe^+$, has $I = 1/2$, $^{131}Xe^+$ has $I = 3/2$. These non-zero nuclear spins cause nuclear spin splitting of the energy levels. This nuclear spin splitting is considerably larger than the isotopic splitting and dominates the shape of the 5d $^4D_{7/2} \rightarrow$ 6p $^4P_{5/2}$ line.

For Xe^+ the total angular momentum is $\boldsymbol{F} = \boldsymbol{J} + \boldsymbol{I}$. The corresponding quantum number F and the z-axis projection component M_F of the total angular momentum have values of $F = J+I, J+I-1, \ldots, |J-I|$ and $M_F = F, F-1, \ldots, -F$. The selection rules for nuclear spin splitting are $\Delta F = [0, \pm 1]$, where ΔF is the difference between the lower (F') and upper (F'') state total angular quantum number with the transition $F'=0 \rightarrow F''=0$ being forbidden. Figure 1b shows that the Xe^+ transition 5d $^4D_{7/2} \rightarrow$ 6p $^4P_{5/2}$ at 605.278 nm has three components for $^{129}Xe^+$ and nine components for $^{131}Xe^+$. The energy of the nuclear spin split levels is calculated using nuclear magnetic dipole and nuclear electric quadrupole interaction constants [7].

The relative intensities of each nuclear-spin split component is evaluated based on F, J and I quantum numbers [8]. The resultant hyperfine splitting of Xe^+ 5d $^4D_{7/2} \rightarrow$ 6p $^4P_{5/2}$ line is shown in Figure 3. The relative intensities of the relevant isotopes without nuclear-spin splitting (black lines) is assumed to be equal to their isotopic abundances. The line intensities of $^{129}Xe^+$ (red lines) and $^{131}Xe^+$ (blue lines) are determined by the product of their isotopic abundances and the relative intensities of the nuclear-spin split components.

2.3. Zeeman splitting

In the case of weak to moderate external magnetic field strengths, the hyperfine structure is further split in $2F+1$ sublevels. By analogy with the fine structure, Zeeman splitting for the $F'=3 \rightarrow F''=2$ transition for $^{129}Xe^+$ (see Figure 4) and $^{131}Xe^+$ yields four π-lines for which $\Delta M_F = 0$ and ten σ-lines for which $\Delta M_F = \pm 1$.

The first order energy contribution is given by:

$$E_Z = M_F \left(g_F \mu_B - g_N \mu_N \right) B \,, \qquad (1)$$

where B is the magnetic field strength, μ_B and μ_N are the Bohr magneton and the nuclear magneton, respectively, and $g_{F,N}$ are the Landé factors. The second term in Eq. (1) can be neglected since $g_N \mu_N = m_p/m_e$ is ~1800 times smaller than $g_F \mu_B$. According to Eq. (1), every hyperfine level will be split into a number of equidistant sublevels, each of which will have an energy splitting proportional to the magnetic field strength:

$$\Delta E_Z \cong (M_{F'} g_{F'} - M_{F''} g_{F''}) \mu_B B \,. \qquad (2)$$

Based on Eq. (2), the calculated Zeeman shifts for a magnetic field strength of 1 kG in the case of hyperfine transition $F'=3 \rightarrow F''=2$ for the $^{129}Xe^+$ isotope are shown in Figure 5. The calculations show that the σ lines are shifted plus and minus relative to the rest frame line position by $\approx 2.4 \times 10^{-3}$ Å; equivalent to a frequency shift ≈0.2 GHz. For the $^{131}Xe^+$ isotope, the σ lines are shifted by $\approx 1.9 \times 10^{-3}$ Å. For even isotopes, the effect is larger. For the most abundant isotope, $^{132}Xe^+$, the calculated shift of the σ lines is 1.8 GHz/kGauss. For laser injection parallel to the external magnetic field, the Zeeman splitting of the hyperfine structures can be safely neglected for ion velocity calculations because the displacement of the $\sigma^{\pm}$ lines from the rest frame line

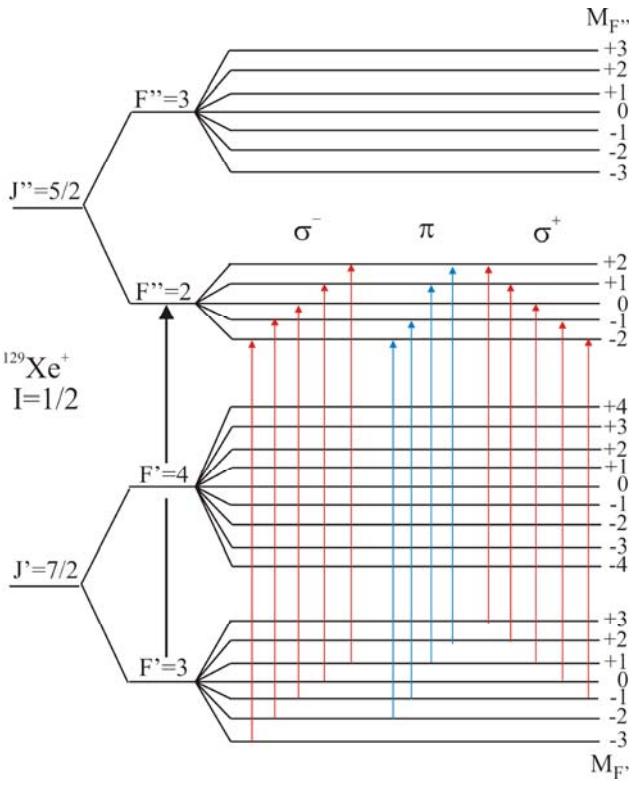

FIG. 4. $^{129}Xe^{+}$ 5d $^{4}D_{7/2}(F'=3) \rightarrow$ 6p $^{4}P_{5/2}(F''=2)$ Zeeman line splitting.

is nearly symmetric; the error introduced by assuming complete Zeeman splitting symmetry is less than a few tens of m/s.

Because the Xe^{+} absorption line is a convolution of hyperfine split lines, each of them Zeeman split, the full width at half maximum (FWHM) of the absorption lineshape is wider than the FWHM in the absence of an external magnetic field, Doppler broadening, i.e., ion temperature, does not dominate the absorption linewidth. For the $^{132}Xe^{+}$ ion, we estimate that Zeeman splitting nearly doubles the observed linewidth. If ion temperature is determined by the simple Doppler broadening approximation:

$$k_B T = (m\lambda_0^2 / 8\ln 2)(\Delta\nu)_{1/2}^2 \qquad (3)$$

where m is the ion mass, λ_0 the rest frame wavelength, $(\Delta\nu)_{1/2}$ the FWHM of the distribution expressed in GHz and k_B is Boltzmann's constant, the Zeeman broadening would lead to a factor of four over-estimation of the ion temperature.

The overlap of the many isotopic and Zeeman split lines makes deconvolution of the Xe^{+} linewidth to obtain the ion temperature extremely difficult, if not impossible. In summary, the natural isotopic composition of xenon and the presence of a non-zero nuclear spin in odd isotopes 129 and 131 results in an Xe^{+} LIF absorption linewidth that spans approximately 8 GHz.

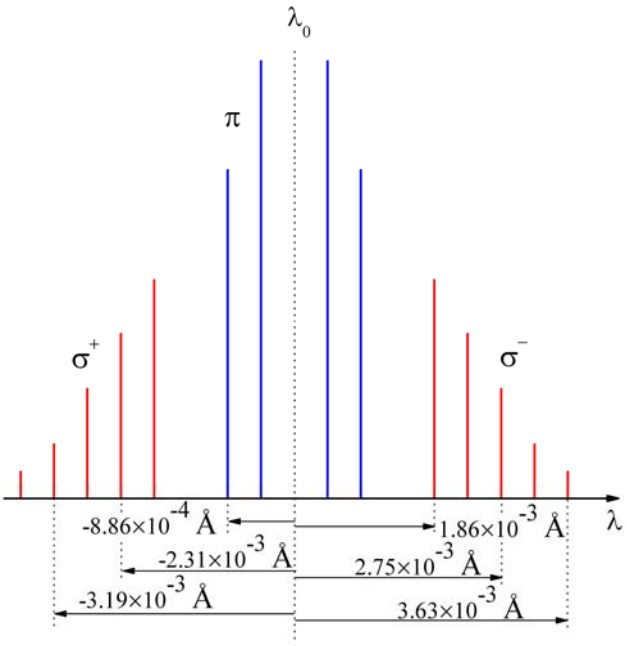

FIG. 5. $^{129}Xe^{+}$ Zeeman shifts for F'=3 → F''=2 hyperfine transition of the λ_0=605.278 nm line.

3. Ion flow velocity calculation

To accurately determine the bulk ion velocity from the LIF measured ivdf, the LIF system must be calibrated in absolute laser frequency. Although the resolution of the Burleigh 1800 wavemeter used in this work is sufficient to tune the dye laser to the appropriate wavelength, the wavemeter refresh rate is too slow for the laser scanning rates typically used for LIF measurements, ~ 0.5 GHz/s.

Therefore an iodine absorption spectrum was recorded for each scan of the laser. To identify the appropriate iodine lines to be used as a zero velocity reference for the LIF measurements, the *Salami* reference iodine spectrum [9] was compared to experimentally obtained iodine spectra in the range of interest for the LIF scheme. As can be seen in Figure 6, for the Xe^{+} 605.2781 nm (16521.33 cm^{-1}) absorption line, the closest iodine line with a sufficient intensity is the 16521.45 cm^{-1} line. Available tables [10] based on early measurements by *Humphrey* [11] provide a value for the Xe^{+} absorption line wave number of 16521.22 cm^{-1}. Based on interferometric measurements, in a later paper [12] *Humphrey* reported an improved value of 16521.285 cm^{-1}. *Hansen and Persson* [13] also reported a wave number of 16521.22 cm^{-1}. The most recent wave number values are by *Sadeghi* [14], who reported a wave number value of 16521.299 cm^{-1} based on Lamb dip spectroscopy and by *Cedolin et al.*[15] who reported a value of 16521.23 cm^{-1} based on direct and reflected LIF. Converted into frequency, the variation between maximum and

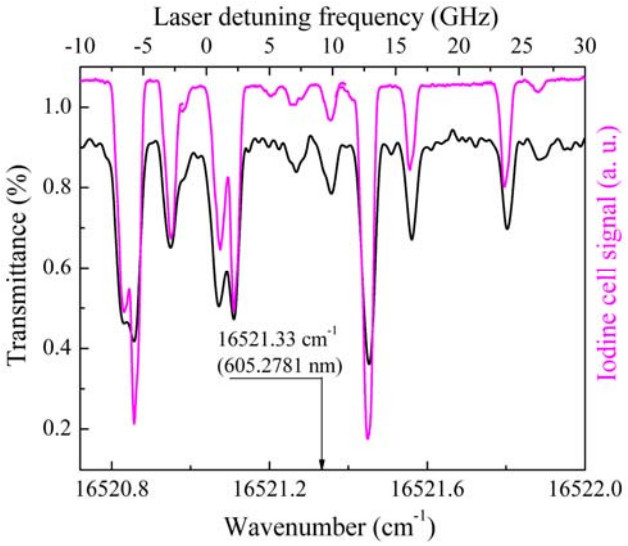

FIG. 6. The experimental iodine spectrum (magenta) and the absorption iodine spectrum (black) according to Ref. [9]. The arrow indicates the absolute wave number of the 605.2781 nm Xe^+ line.

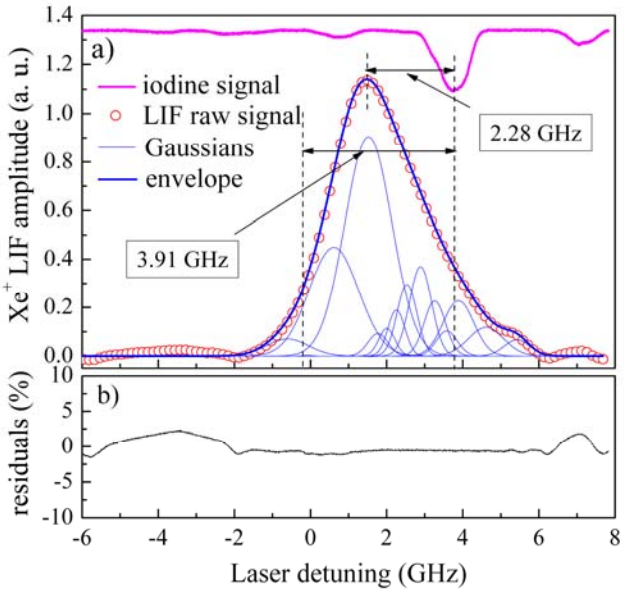

FIG. 7. Parallel LIF measurement of Xe^+: the red symbols are the raw LIF signal, the blue thin lines are Gaussian fits to the 15 components, the blue thick line is the envelope of the fits, and the magenta line is the iodine reference spectrum.

minimum reported wave number values (~0.08 cm^{-1}) spans 2.4 GHz. Because the ion velocity is given by

$$V \cong \lambda_0 \Delta \nu_{total} \quad (4)$$

where the velocity V is in m/s if the rest frame wavelength λ_0 is in nm and the frequency shift $\Delta \nu_{total}$ is in GHz, it follows then this uncertainty corresponds to an ion velocity uncertainty of ≈1.5 km/s. Therefore, measurements of the perpendicular (to the magnetic field) Xe^+ ivdf in stationary plasma were used to determine that the zero velocity reference wave number of the absorption line is 16521.332 cm^{-1}. The frequency difference between the reference iodine line and the rest frame Xe^+ 605.2781 nm absorption line is therefore 3.91 GHz.

In actual practice, determination of the absolute shift of the peak of the Xe^+ absorption line (associated with the ^{132}Xe isotope due to its largest natural abundance) relative to the reference iodine spectrum requires subtraction of 3.91 GHz offset from the measured frequency shift of the LIF measurement peak, e.g., 2.28 GHz in Fig. 7. As shown in Figure 7, the LIF measured Xe^+ lineshape is clearly non-Gaussian. Because four of the hyperfine structures are too weak (< 0.1 relative intensity) to include in the overall LIF profile, a deconvolution of the Xe^+ LIF line with only fifteen Gaussian profiles centered at each of the fifteen component hyperfine line centers was performed. Deconvolution yields excellent agreement between the overall envelope and the raw LIF measurement; the residuals being below 3%. However, the integrated line shapes generated by the deconvolution fit parameters are inconsistent with the expected relative intensities and the FWHMs generated by the deconvolution are not equal one to each other (which is thermodynamically implausible). Thus, as noted previously, the bulk ion velocity can be determined with considerable precision but the ion temperature cannot be uniquely determined.

4. Helicon Source Electric Fields and Mode Transitions

Once the details of the Xe^+ LIF scheme were established, LIF measurements were used to determine the axial electric field downstream of the antenna in a helicon discharge. Details of the helicon plasma source are given elsewhere [16, 17]. LIF measurements of the xenon ivdf were obtained as a function of rf power at two axial positions, z = 90 cm and z = 110 cm downstream from the antenna (a half wave, 19 cm long, m=+1 helical antenna). The rf driving frequency was 9.5 MHz, and the magnetic field strengths in the source and expansion chamber were 700 G and 10 G, respectively. The mass flow rate was 8 sccm for which the pressure in the vicinity of gas inlet was 1.3 mTorr.

As shown in Figure 8a, over the rf power range of 350-750 W, parallel ion flow velocities at the axial two locations, 0.8 km/s and 1.5 km/s, respectively, are independent of the rf power. Since the estimated neutral axial flow speed based on the known neutral

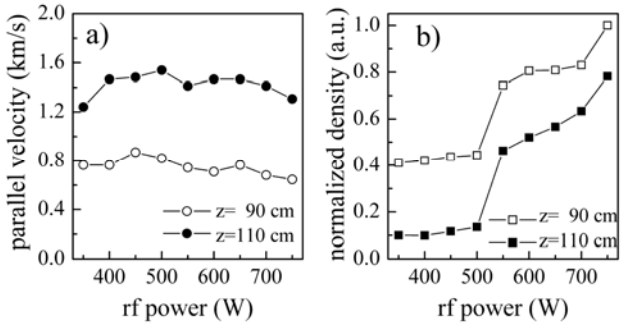

FIG. 8. a) Xe^+ parallel flow speed and b) the normalized Xe^+ density estimated from the LIF signal amplitude.

gas pressure gradient is at most ≈ 0.4 km/s, the measured difference of xenon ion speed is likely due to ambipolar diffusion along the magnetic field. After subtracting the estimated neutral gas flow speed, the calculated potential difference between those locations is 0.5 V, i.e., a 2.5 V/m axial ambipolar electric field.

Under the assumption that the main population mechanism of the Xe^+ 5d $^4D_{7/2}$ metastable level interrogated via LIF is electron impact excitation from the ion ground state, LIF signals in helicon plasmas have been found to be roughly proportional to a composite parameter given by the square of the electron density times the square root of the electron temperature [18]

$$I_{LIF} \sim n_e n_i T_e^{1/2} \cong n_e^2 T_e^{1/2} \qquad (5)$$

This proportionality also assumes that cascading effects from upper states do not contribute significantly to the interrogated metastable state population. Although it is not an absolute calibration, Eq. (5) provides a qualitative correlation between the LIF signal (the metastable ion population) and the ground state ion population (assumed to be equal to the electron density). The square root of the Xe^+ LIF signal amplitude as a function of rf power is shown in Figure 8b. Since the electron temperature is roughly constant for the different input rf powers, the square root of LIF signal amplitude is a qualitative indicator of the trend Xe^+ density. To isolate the dependance of the ion density evolution on the input rf power, the LIF signals at both locations were normalized to maximum value (corresponding to highest power level for the closest position to the antenna). With increasing rf power, a significant jump in ion density at 550 W is observed at both locations.

This density jump corresponds to a discharge mode change from electrostatic (E mode) to inductive (H mode). A second density jump that might be associated with an inductive to helicon (W mode) mode transition is also observed around 750 W. The similarity in the ion density trends at both two axial locations and the fact that more than 100 cm downstream from the antenna the LIF signal still "feels" the changes in rf coupling modes provides further confidence in the use of the LIF signal as a qualitative indicator of ion density.

5. References

[1] D. Gawron, S. Mazouffre, N. Sadeghi, and A. Heron, Plasma Sources Sci. Technol. **17** (2008) 025001

[2] G. J. Williams Jr., T. B. Smith, M. T. Domonkos, A. D. Galimore, and R. P. Drake, IEEE Trans. Plasma Sci. **28** (2000) 1664

[3] L. Broström, S. Mannervik, A. Passian, and G. Sundström, Phys. Rev. A **49** (1994) 3333

[4] S. Mannevrik, L. Broström, J. Lidberg, L. O. Norlin, and P. Royen, Phys. Rev. Lett. **76** (1996) 3675

[5] E. Browne, *Table of Isotopes*, Edts. C. M. Lederer and V. S. Shirley, 7-th ed., Wiley (1978)

[6] C. R. Bingham *et al*., Nuclear Instr. and Methods **202** (1982) 147

[7] R. A. Holt, S. D. Rosner, and T. D. Gaily, Phys. Rev. A **15** (1997) 2293

[8] H. E. White, *Introduction to Atomic Spectra,* McGraw-Hill Book Company (1934)

[9] H. Salami and A. Ross, J. Molec. Spectr. **233** (2005) 157

[10] http://physics.nist.gov/PhysRefData/ASD/index.htm

[11] C. J. Humphrey, J. Res. Nat. Bur. Stand. **23** (1939) 683

[12] C. J. Humphrey, J. Opt. Soc. Am. **60** (1970) 1454

[13] J. E. Hansen and W. Persson, Phys. Scripta **36** (1987) 602

[14] N. Sadeghi, N. Dorval, J. Bonnet, D. Pigache, C. Kadlec-Philippe, and A. Bouchoule, The 35-th AIAA/ASM/SAE/ ASEE/ *Joint Propulsion Conference & Exhibit*, June 20-23, Los Angeles, CA (1999)

[15] R. J. Cedolin, W. A. Hargus Jr., P. V. Storm, R. K. Hanson, and M. A. Cappelli, Appl. Phys. B **65** (1997) 459

[16] I. A. Biloiu, E. E. Scime, and C. Biloiu, Appl. Phys. Lett. **92** (2008) 191502

[17] I. A. Biloiu, E. E. Scime, and C. Biloiu, Plasma Sources Sci. & Technol. **18** (2009) 025012

[18] E. Scime, R. Hardin, C. Biloiu, A. Keesee, and X. Sun, Phys. Plasmas **14** (2007) 043505